Synchronization of spin torque nano-oscillators

James Turtle,[1,*] Pietro-Luciano Buono,[2,†] Antonio Palacios,[1,‡] Christine Dabrowski,[2,§] Visarath In,[3,‖] and Patrick Longhini[3,¶]
[1]*Nonlinear Dynamical Systems Group, Department of Mathematics, San Diego State University, San Diego, California 92182, USA*
[2]*Faculty of Science, University of Ontario Institute of Technology, 2000 Simcoe Street North, Oshawa, Ontario, Canada L1H 7K4*
[3]*Space and Naval Warfare Systems Center Pacific, Code 71730, 53560 Hull Street, San Diego, California 92152-5001, USA*
(Received 12 October 2016; revised manuscript received 17 March 2017; published 12 April 2017)

Synchronization of spin torque nano-oscillators (STNOs) has been a subject of extensive research as various groups try to harness the collective power of STNOs to produce a strong enough microwave signal at the nanoscale. Achieving synchronization has proven to be, however, rather difficult for even small arrays while in larger ones the task of synchronization has eluded theorists and experimentalists altogether. In this work we solve the synchronization problem, analytically and computationally, for networks of STNOs connected in series. The procedure is valid for networks of arbitrary size and it is readily extendable to other network topologies. These results should help guide future experiments and, eventually, lead to the design and fabrication of a nanoscale microwave signal generator.

DOI: 10.1103/PhysRevB.95.144412

I. INTRODUCTION

The synchronization phenomenon of spin torque nano-oscillators (STNOs) has been the subject of extensive research for many years due to the potential of networks of STNOs to generate microwave signals at the nanoscale [1–3]. In the last few years, Adler-type [4] injection locking has emerged as the most promising method to achieve synchronization, either through an external microwave current [5–7] or through a microwave magnetic field [8,9]. In particular, it was shown recently that a record number of five nanocontact STNOs [10] can synchronize via spin-wave beams [11]. Non-Adlerian approaches to synchronization of nanopillar STNOs have also been considered. Georges *et al.* [12] found the critical coupling strength and minimum number of STNOs for the onset of synchronization analytically by describing the STNOs as phase oscillators in the framework of Kuramoto [13]. Later, Iacocca and Akerman [14] provided conditions for the onset of phase instability that may be caused, surprisingly, by strong coupling in identical STNOs. It is well known, however, that amplitude can affect synchronization, especially near the onset of a Hopf bifurcation [15]. In fact, in STNOs amplitude and phase are intrinsically coupled by the dependence of the effective field on the magnetization [16]. Thus, if the Hopf bifurcation parameter is of the same scale as the coupling parameter then the amplitude is no longer negligible and the Kuramoto model reduction is no longer valid. Furthermore, when the amplitude dynamics are not negligible and the natural oscillation frequencies are not homogeneous, synchronization may be enhanced regardless of the topology of the network [17]. Consequently, a complete understanding of synchronization of nanopillar-based STNOs, via non-Adlerian type, requires an analysis that incorporates the amplitude dynamics.

In 2005, back-to-back publications in *Nature Letters* (Kaka [2], a collaboration between NIST and Hitachi GST and Mancoff [18] from Freescale Semiconductor) showed that two STNOs tend to phase lock when they are in close proximity of one another. The coupling in these cases resulted from spin waves propagating through the continuous free layers, leading to phase locking. Soon after, Grollier *et al.* [1] investigated computationally the behavior of a one-dimensional (1D) series array of $N = 10$ electrically coupled STNOs. Their study showed that the ac produced by each individual oscillator leads to feedback between the STNOs, causing them to synchronize, and that, collectively, the microwave power output of the array increases as N^2. In a follow-up study, Persson *et al.* [3] mapped out numerically the region of synchronization of the 1D serially connected array considered by Grollier *et al.* for the special case of $N = 2$ STNOs. Their work shows that the region of parameter space where synchronization exists is rather small, thus explaining the difficulty (already observed by experimentalists) to achieve synchronization. Li *et al.* [19] showed that this difficulty was due, mainly, to the coexistence of multiple stable attractors, suggesting that the synchronization regime is highly sensitive to initial conditions. Persson *et al.* [3] also investigated numerically the effect of including a time delay between the magnetization-induced change in voltage and the current variation. They highlight that this increases significantly the parameter region of synchronization, especially with respect to differences in anisotropy fields between the STNOs. We determine numerically that the synchronization for 1000 STNOs is robust to nonhomogeneities in the anisotropy field on the order of 4–5%, as Persson *et al.* also observes in the absence of delay. It will be worthwhile to investigate in future work the effects of time delay and to find out whether the synchronization is robust to larger anisotropy in the network.

On a single STNO [see Fig. 1(a)], an originally unpolarized electric current I, in amperes, is applied to the fixed magnetic layer whose magnetization is represented by $\hat{M}$. As the electrons pass through the layer, their spins become aligned to that of the fixed layer, thus creating a *spin-polarized* current. Then the polarized current exerts a torque on the magnetization of the free layer, which can lead to steady precession. We

*jturtle@predsci.com
†Pietro-Luciano.Buono@uoit.ca
‡apalacios@mail.sdsu.edu
§christinedabrowski15@gmail.com
‖visarath@spawar.navy.mil
¶patrick.longhini@navy.mil

 ©2017 American Physical Society

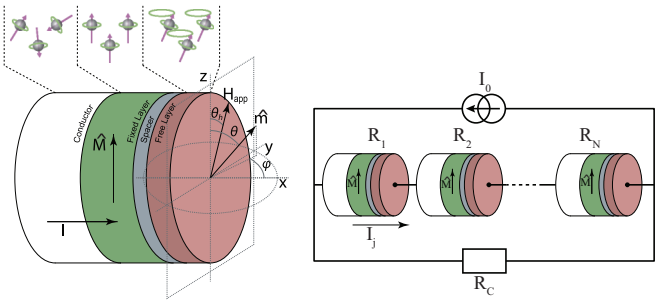

FIG. 1. Left: Schematic representation of a nanopillar STNO. A spin-polarized current can exert a torque on the magnetization of the free layer and lead to steady precession. Right: A circuit array of STNOs connected in series.

consider a circuit array of N identical STNOs coupled in series [see Fig. 1(b)] and study the conditions to synchronize the individual precessions. Our approach employs the dc current, $I_{\rm dc}$, flowing in each STNO and the angle θ_h of the applied magnetic field as the bifurcation parameters. No injection of ac current is required. The all-to-all coupling of the network of identical STNOs implies a complete permutation symmetry which we exploit using equivariant bifurcation theory [20].

We search for fully synchronized periodic oscillations in the network of N STNOs, first by finding implicit analytical expressions for Hopf bifurcation curves, in $(I_{\rm dc},\theta_h)$ space, at a synchronized equilibrium that yield symmetry-preserving in-phase oscillations (see Fig. 2). We calculate the stability of the synchronization manifold near a synchronous equilibrium and combine Hopf criticality results to determine regions of parameter space where the fully synchronized periodic state is asymptotically stable near bifurcation. More importantly, the results are valid for networks of arbitrary size N. Normal hyperbolicity [22,23] guarantees the synchronization manifold is robust to small nonhomogeneities in the STNOs. Numerical simulations show that synchronization is preserved to approximately $\pm 5\%$ variations in anisotropy strength. Results are illustrated with arrays of up to $N = 1000$ nano-oscillators (see Fig. 3). The analysis also captures symmetry-breaking patterns of oscillations, but we do not pursue the study of those cases here. These patterns are described as "multiple synchronization attractors" in Ref. [24].

II. LOCI OF STABLE SYNCHRONIZED OSCILLATIONS

The free-layer magnetization vector, $\hat{m} = [m_1,m_2,m_3]^T$, for an individual nanopillar oscillator is governed by the Landau-Lifshitz-Gilbert-Slonczewski (LLGS) [25–28] equation

$$\frac{d\hat{m}}{dt} = -\gamma\, \hat{m} \times \vec{H}_{\rm eff} + \alpha\, \hat{m} \times \frac{d\hat{m}}{dt} - \gamma\, \mu\, I \hat{m} \times (\hat{m} \times \hat{M}), \tag{1}$$

where γ is the gyromagnetic ratio, α is the Gilbert damping term, μ contains material parameters, and $\vec{H}_{\rm eff}$ is the effective magnetic field. The term $\vec{H}_{\rm eff}$ consists of an anisotropy field, $\vec{H}_{\rm an} = \kappa(\hat{m}\cdot\hat{e}_{||})\hat{e}_{||}$, where κ is the strength of the anisotropy (we set $\kappa = 45$ Oe in our simulations [21]) and $e_{||} = [\sin\theta_{||}\cos\phi_{||}, \sin\theta_{||}\sin\phi_{||}, \cos\theta_{||}]^T$ is a preferred direction of

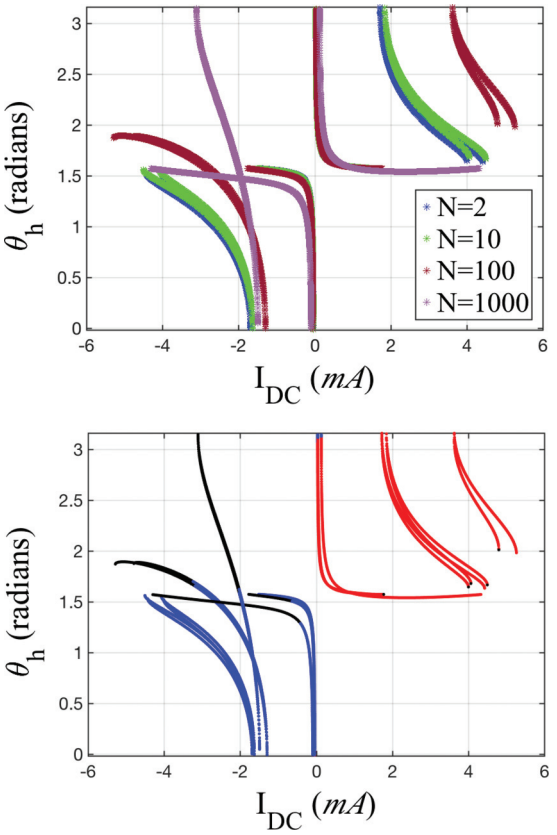

FIG. 2. Top: Loci of Hopf bifurcations of synchronized oscillations. Bottom: Stability of synchronization manifold (red, supercritical Hopf and stable synchronization manifold; black, subcritical Hopf and unstable synchronization manifold; and blue, supercritical Hopf and unstable synchronization manifold). The combined results of these two plots reveal the optimal region to synchronize a series array of nanopillar STNOs: the first quadrant of parameter space $(I_{\rm dc},\theta_h)$. Parameters [21] are $N_1 = 1$, $N_2 = 0$, $\gamma = 2.2\times10^5\,{\rm m\,A^{-1}\,s^{-1}}$, $\alpha = 0.008$, $\kappa = 45$ Oe, $\mu = 0.992$, $h_a = 300$ Oe, $\beta_{\triangle R} = 5.95\times10^{-4}$.

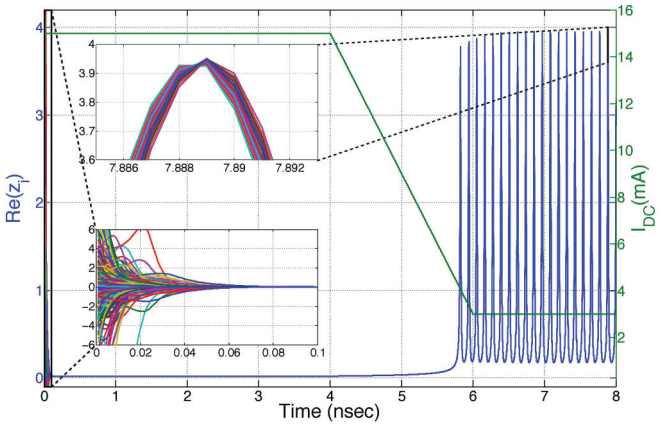

FIG. 3. Locking into synchronization with $N = 1000$ STNOs. Start at high $I_{\rm dc}$ and let the system lock into the common equilibrium. Then sweep down $I_{\rm dc}$ until the common equilibrium vanishes and synchronized oscillations appear. Top inset: Zoom-in on the top part of the oscillation showing a high level of synchronization between all the STNOs. Bottom inset: Zoom-in on the set of random initial conditions for the $N = 1000$ STNOs and evolution for small time values showing rapid convergence to a synchronized equilibrium.

magnetization. $\vec{H}_{\rm d}$ is a demagnetization field and we set $\vec{H}_{\rm d} = -4\pi S_0(N_1 m_1 \hat{x} + N_2 m_2 \hat{y} + N_3 m_3 \hat{z})$, where $S_0 = 8400/4\pi$ is the constant magnitude of the average magnetization vector $S(t)$ (in units of oersted) so that $\hat{m} = S/S_0$, N_1, N_2, and N_3 are dimensionless constants satisfying $N_1 + N_2 + N_3 = 1$, and $\{\hat{x},\hat{y},\hat{z}\}$ are the orthonormal unit vectors. $\vec{H}_{\rm appl}$ is an applied magnetic field given by $\vec{H}_{\rm appl} = h_a\,[0, \sin\theta_h, \cos\theta_h]^T$, which we assume to lie on the yz plane at some angle θ_h instead of the z axis, and note that h_a is in units of oersted. $\hat{M}$ is the fixed-layer magnetization vector that defines the spin-polarization direction of the current. In what follows we assume $\theta_{||} = 0$ so that $e_{||} = [0,0,1]$, which produces an easy axis in the z direction. Finally, we assume the direction of polarization of the spin-polarized current to remain constant along the z direction, i.e., $\hat{M} = \hat{z}$.

For an array of STNOs, coupling occurs if the input current I is replaced by I_j. First, we assume the STNOs to be identical. Later, we consider the effects of nonhomogeneities as perturbations of the synchronization manifold. Applying Kirchhoff's laws we obtain the current through the jth STNO:

$$I_j = I_{\rm dc}\left(1 + \sum_{i=1}^{N} \beta_{\Delta Ri}\cos\theta_i(t)\right), \tag{2}$$

where $I_{\rm dc}$ is a constant dc, $\beta_{\Delta Ri}$ is a parameter that depends on the resistances in the parallel and antiparallel magnetization states, and $\theta_i(t)$ is the angle between the magnetization of the fixed and free ferromagnetic layers. We substitute Eq. (2) into Eq. (1) and, for convenience, we convert to complex stereographic coordinates through the change of variables $z_j = (m_{j1} + i m_{j2})/(1 + m_{j3})$. Direct calculations yield

$$\dot{z}_j = \frac{\gamma(1+i\alpha)}{1+\alpha^2}\Bigg[ih_{a_3}z_j + \frac{h_{a_2}}{2}\left(1+z_j^2\right) + i\kappa\frac{1-|z_j|^2}{1+|z_j|^2}z_j - \mu I_{\rm DC}z_j - \mu I_{\rm DC}\beta_{\Delta R}\sum_{k=1}^{N}\frac{1-|z_k|^2}{1+|z_k|^2}z_j$$
$$- \frac{4\pi S_0}{1+|z_j|^2}\left(\frac{N_1-N_2}{2}\left(z_j^3 - \bar{z}_j\right) + \left(1 - \frac{3N_1+3N_2}{2}\right)\left(z_j - z_j|z_j|^2\right)\right)\Bigg], \tag{3}$$

where $h_{a_2} = h_a\sin(\theta_h)$ and $h_{a_3} = h_a\cos(\theta_h)$.

For the special case $N_1 = N_2 = 0.5$, Eq. (3) is more amenable to analysis, and thus we can find, via MAPLE, implicit analytic expressions for the Hopf loci that yield synchronized periodic states for arbitrary arrays of size N. Although the synchronized periodic oscillation is unstable, we can still use these analytical expressions to follow, via the automatic numerical continuation software AUTO [29], the movement of the Hopf loci as a function of the continuation parameter s, where $N_1 = 0.5 + s$ and $N_2 = 0.5 - s$. For $s = 0.5$, we arrive at the physically relevant configuration of easy-plane anisotropy or x-axis demagnetization. The Hopf loci curves for $s = 0.5$ are shown in Fig. 2 (top) for various sizes of networks. In addition, we determine the criticality of each Hopf loci point through the Lyapunov constant formula [30] as well as the local asymptotic stability of the synchronization manifold near the Hopf point, via AUTO. This process yields, for $s = 0.5$, the red Hopf loci curves located in the first quadrant of $(I_{\rm dc},\theta_h)$ space from which stable synchronized periodic solutions bifurcate (see Fig. 2, bottom).

Observe that the location of these curves implies that less current is required to synchronize larger arrays. This observation suggests that synchronization in series arrays of nanopillar STNOs depends more on the dynamical parameters than on the coupling strength. Similar results have been observed in studies of power grids, which can also be treated as Kuramoto oscillator networks [31].

We wish to emphasize that the aim of this paper is strictly the theoretical analysis to determine regions of existence of stable synchronization. Effects of noise, such as linewidth reduction, are briefly addressed in Sec. VII, but a detailed analysis is ongoing and deferred to a future publication. Next we present an outline of the analysis that was carried out to obtain the implicit solutions of the Hopf loci.

III. HOPF BIFURCATION CURVES

This section summarizes the mathematical analysis of how one can exploit the symmetry of the network to obtain the main results shown in Fig. 2. Details of these calculations can be found in Appendix.

Due to the all-to-all coupling that appears in Eq. (3) as a consequence of Kirchhoff's law, and the assumption of identical STNOs, any permutation of the STNOs in the array leaves the coupling term invariant; thus, the series array has symmetry group $\mathbf{S}_N$, the group of all permutations of N objects. To find analytical expressions for the Hopf loci of synchronized solutions we study the linearized system near the origin. Let $\mathbf{z} = (z_1,\ldots,z_N) \in \mathbb{C}^N$ and denote Eq. (3) by $\dot{z}_j = f_j(\mathbf{z})$. Since we assume all the STNOs to be identical, we have $f_1 = f_2 = \cdots = f_N$. We rewrite the system of Eq. (3) in abbreviated form

$$\dot{\mathbf{z}} = \mathbf{f}(\mathbf{z}), \tag{4}$$

where $\mathbf{f} = [f_1,\ldots,f_N]^T$. Let $\mathbf{z}_0 = (z_0,\ldots,z_0)$ be an equilibrium solution of Eq. (4) with isotropy subgroup $\mathbf{S}_N$ [20]. Then the linearization at $\mathbf{z}_0$ is given by

$$\mathbf{L} := \begin{bmatrix} \mathbf{A} & \mathbf{B} & \cdots & \mathbf{B} \\ \mathbf{B} & \ddots & \ddots & \vdots \\ \vdots & \ddots & \ddots & \mathbf{B} \\ \mathbf{B} & \cdots & \mathbf{B} & \mathbf{A} \end{bmatrix}, \tag{5}$$

where $\mathbf{A} = (df_{jj})_{\mathbf{z}=\mathbf{z}_0}$ and $\mathbf{B} = (df_{jk})_{\mathbf{z}=\mathbf{z}_0}$ are 2×2 Jacobian matrices of f_j, with $j \neq k$. Using symmetry methods, we block-diagonalize $\mathbf{L}$ to a form which respects symmetry-invariant subspaces. Let P be the change-of-coordinates matrix. Applying P to $\mathbf{L}$, we obtain a block diagonalization of

the linear part of the coupled STNO array,

$$\widetilde{\mathbf{L}} := P^{-1}\mathbf{L}P = \mathrm{diag}\{\mathbf{A}+(N-1)\mathbf{B},\mathbf{A}-\mathbf{B},\ldots,\mathbf{A}-\mathbf{B}\}. \tag{6}$$

From the diagonal structure, the eigenvalues of the blocks are also eigenvalues of $\widetilde{\mathbf{L}}$. It follows that Hopf bifurcations in Eq. (4) occur if and only if $\mathbf{A}+(N-1)\mathbf{B}$ or $\mathbf{A}-\mathbf{B}$ have purely imaginary eigenvalues. In the former case, the eigenspace associated with $\mathbf{A}+(N-1)\mathbf{B}$ is $v_0=[v,\ldots,v]^T$ and the symmetry group $\mathbf{S}_N$ acts trivially on v_0. This corresponds to a symmetry-preserving Hopf bifurcation in which all STNOs oscillate in synchrony, i.e., the same wave form, same amplitude, and same phase. In the latter case, the eigenvalues have, generically, multiplicity $N-1$ (from the $N-1$ blocks $\mathbf{A}-\mathbf{B}$) and the emerging patterns of oscillations arise via symmetry-breaking Hopf bifurcations [20]. For instance, the case reported in Ref. [24], in which two pairs of STNOs are in phase with one another and half a period out-of-phase with respect to each pair, corresponds to a Hopf symmetry-breaking pattern that emerges from the $\mathbf{A}-\mathbf{B}$ block with $N=4$. A complete description of the possible patterns of oscillations that can appear for each value of N can be found via equivariant Hopf bifurcation [20]. The emphasis of this paper is, however, on the symmetry-preserving synchronization state.

Combining the equilibrium conditions with the trace condition of purely imaginary eigenvalues for the block $\mathbf{A}+(N-1)\mathbf{B}$ and using polar coordinates, $z_0=r(\cos\theta+i\sin\theta)$, we get the following set of equations as a function of $(r,\cos\theta,I_{\mathrm{dc}},\theta_h)$:

$$\begin{aligned}\mathrm{Re}(f_j)&=0\\ \mathrm{Im}(f_j)&=0\\ \mathrm{Tr}(\mathbf{A}+(N-1)\mathbf{B})&=0.\end{aligned} \tag{7}$$

To find the desired analytical expressions for the Hopf boundary curves, we solve Eqs. (7) implicitly for the state variables (r,θ) as functions of the parameters I_{dc} and θ_h. We set $N_1=N_2=0.5$ as a starting point to facilitate the analysis. Through a series of substitutions we are able to reduce this system of three equations with four unknowns, $(r,\theta,I_{\mathrm{dc}},\theta_h)$, to a single expression with two variables (r,θ_h). To plot the boundary curves, we first extract the coordinate points from the solution sets, and back-substituting gives the actual point values $(I_{\mathrm{dc}},\theta_h)$ along the curves. Varying N we can then trace the movement of the synchronous Hopf bifurcation curves. We verify along the curves obtained that $\det(\mathbf{A}-\mathbf{B})>0$ and $\det(\mathbf{A}+(N-1)\mathbf{B})>0$. The results just described are then extended using AUTO to the case $N_1=1$, $N_2=N_3=0$ by continuing the Hopf loci curves in $(I_{\mathrm{dc}},\theta_h)$ space using $N_1=0.5+s$ and $N_2=0.5-s$ and letting the continuation parameter s evolve from 0 to 0.5.

IV. STABILITY

The Hopf bifurcation can be supercritical or subcritical, leading to stable or unstable synchronized oscillations, respectively. Which one appears is determined by the Lyapunov constant [30]. If the Lyapunov constant is negative, the Hopf bifurcation is supercritical, whereas if it is positive, it leads to a subcritical Hopf bifurcation. Now, the stability property of the synchronization manifold is determined by the eigenvalues transverse to the manifold. Those eigenvalues are given by $N-1$ copies of the eigenvalues of the block $\mathbf{A}-\mathbf{B}$ and since the synchronization manifold is computed near an equilibrium, then normal hyperbolicity follows from the eigenvalues of the $\mathbf{A}-\mathbf{B}$ block. The actual calculations of the Lyapunov constant and that of the transverse eigenvalues are technical and lengthy and appear in Appendix under nonlinear analysis.

V. LOCKING INTO SYNCHRONIZATION

Numerical simulations indicate the common equilibrium state of large arrays has a large basin of attraction for large values of dc, about 15 mA. This suggests a possible strategy to achieve synchronization in actual experiments: start the experiments at high I_{dc} current and let the system lock into the common equilibrium. Then sweep down I_{dc} until the common equilibrium vanishes at a saddle-node bifurcation and stable synchronized oscillations appear, created via Hopf bifurcation from a coexisting common equilibrium found at lower I_{dc} values. This strategy was tested with nonhomogeneities introduced through variations in the anisotropy field constant κ. As a consequence of the normal hyperbolicity of the synchronization manifold, we expect the synchronization state to be robust under small perturbations, such as the nonhomogeneities in κ. Indeed, numerical simulations confirm that the STNOs are able to synchronize with up to $\pm5\%$ variations in anisotropy strength if the values are chosen randomly from a uniform distribution (see Fig. 3), and up to $\pm4\%$ with a Gaussian distribution.

VI. FREQUENCY RESPONSE

We now employ the fast Fourier transform (FFT) to characterize the frequency response in networks of N nonidentical oscillators coupled in series. The plots in Fig. 4 show the frequency of oscillation for $N=1$, 10, 100, and 1000. The observed "dips" for small values of I_{dc} correspond to the switch from out-of-plane oscillations to in-plane oscillations.

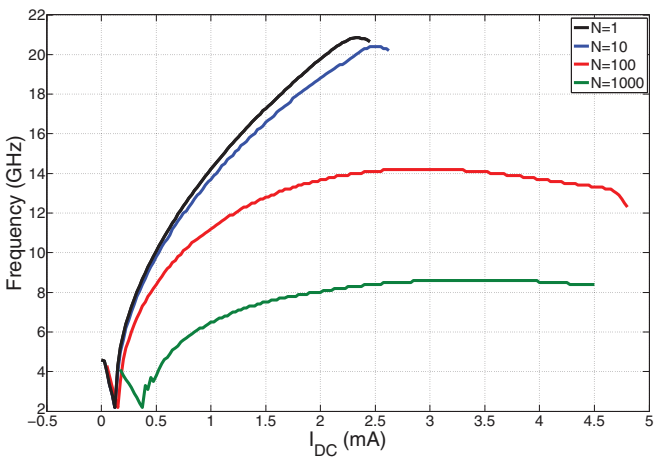

FIG. 4. Frequency response of an array of N STNOs connected in series. The observed dips in frequency correspond to switching between out-of-plane and in-plane oscillations. Parameters are the same as in Fig. 2, with $\theta_h=3\pi/4$.

For $\theta_h = 0$, the switch is characterized by a gluing bifurcation, that is, a global bifurcation where a pair of homoclinic loops (symmetrically related in this case) are connected to a saddle equilibrium; see Ref. [32] for an example in the context of STNOs. For $\theta_h = 3\pi/4$, which is the value used in Fig. 4, the switch involves two homoclinic bifurcations. In both cases, the switch from out-of-plane to in-plane oscillations explains why the frequency approaches 0 Hz. In general, lines terminating at nonzero frequency correspond to known Hopf bifurcations, and lines terminating at or near 0 Hz correspond to suspected (not verified for every value of N) homoclinic bifurcations. These results suggest that the range of I_{dc} values for which oscillations are present increases with the number of STNOs; however, the interval of possible frequencies decreases with increased N.

VII. LINEWIDTH

We now consider (briefly) the effects of thermal noise on the oscillations of the synchronized solutions by adding a stochastic thermal field term $\vec{H}_{\rm th}$ to $\vec{H}_{\rm eff}$ [33,34] in the original LLGS Eq. (1), becoming

$$\frac{d\hat{m}}{dt} = -\gamma\, \hat{m} \times (\overrightarrow{H}_{\rm eff} + \overrightarrow{H}_{\rm th}) + \alpha\, \hat{m} \times \frac{d\hat{m}}{dt} - \gamma\, \mu\, I \hat{m} \times (\hat{m} \times \hat{M}), \tag{8}$$

where $\overrightarrow{H}_{\rm th} = [h_x(t), h_y(t), h_z(t)]^T$, in which $h_x(t)$, $h_y(t)$, and $h_z(t)$ are Gaussian distributed random functions, uncorrelated, of zero mean. The added term also carries to the complex form of Eq. (3). Linewidth was computed as full width of the power spectral decomposition (PSD) of the synchronized oscillations, via FFT, at half maximum of main frequency in the PSD. The computation was carried out as a function of I_{dc}, on the same interval of the frequency response of Fig. 4, and for a few different values of array size N. The results are shown in Fig. 5.

The spikes in linewidth that are observed near the end points of the interval of synchronization are due to the oscillations having different characteristics. More specifically, for small I_{dc} the spikes are due to a change to out-of-plane oscillations and for large I_{dc} (and large arrays) the spikes are due to loss of synchronization; i.e., for large arrays the synchronized oscillations give way to out-of-phase oscillations before eventually converging to an equilibrium point. But for the most part of the interval of synchronization, the linewidth remains relatively small. These results suggest, again, that the synchronized solution is significantly robust against the effects of noise. However, one would have to carry out a complete analysis of the stochastic properties of the coupled network equations as a function of coupling strength and noise intensity, for instance. We also wish to point out that temperature is assumed to be implicitly included in the stochastic thermal field. Future experimental works should provide a more explicit contribution of temperature variations and material properties towards the stochastic field. Those issues are important but they are beyond the scope of the present work. Instead, our emphasis is, mainly, on finding the conditions for the existence and stability of synchronized oscillations in the deterministic system. We expect to carry out the stochastic analysis in future work. In particular, it would be interesting to obtain theoretical formulas (possibly asymptotic for large N) for the half linewidth for serially coupled STNOs using the theory developed by Slavin and Tiberkevich [34].

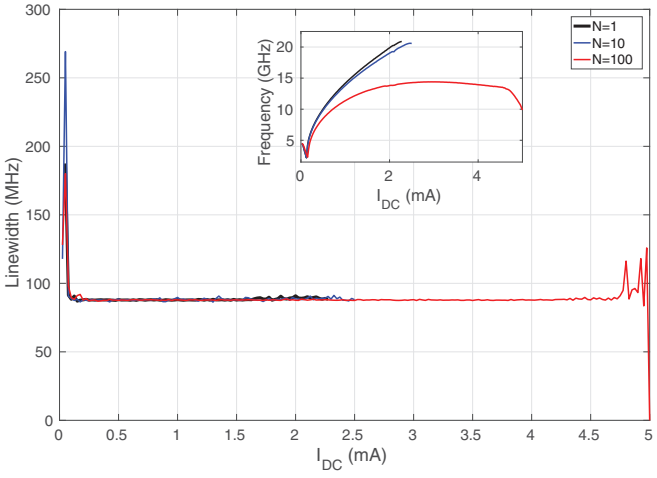

FIG. 5. Linewidth. The observed dips in frequency correspond to switching between out-of-plane and in-plane oscillations. Parameters are the same as in Fig. 2, with $\theta_h = 3\pi/4$.

VIII. DISCUSSION AND CONCLUSIONS

To date, the strongest microwave power that has been produced by a single STNO is on the order of 0.28 μW [35]. As mentioned in the introduction, Grollier *et al.* [1] showed that for an array of $N = 10$ electrically coupled STNOs, the synchronized array microwave power output increases as N^2. Thus, if the N^2 law holds in general, 1000 synchronized nano-oscillators, as simulated in this paper, should produce about 0.28 W. Communication systems, which require power on the order of milliwatts, e.g., wireless devices, radar, air traffic control, weather forecasting, and navigation systems, would only require about 188 nano-oscillators.

In Ref. [32], we showed computationally the nature of the bifurcations leading to these attractors and discovered that changing the angle of the applied magnetization field could enlarge the basin of attraction of the synchronized oscillations. In this work we extended the bifurcation analysis of nanopillar-based STNOs connected in series arrays of arbitrary size. We use equivariant bifurcation theory to find the region of existence and stability of the synchronization manifold for which all STNOs oscillate with the same frequency, phase, and amplitude. Our approach to achieve synchronization, via non-Adlerian dynamics, employs only the dc flowing in each STNO and the angle of the applied magnetic field. The main results include implicit solutions of the Hopf loci as a function of the dc and the applied magnetic field. Normal hyperbolicity of the synchronization manifold implies robustness of the synchronization state to small perturbations, such as those caused by nonhomogeneities or imperfections during the manufacturing process. Computer simulations with nonidentical STNOs indicate robustness up to $\pm 5\%$ variations, which is well within typical fabrication processes. It is our hope that the theoretical results and simulations provided in

this paper will help guide ongoing experiments. The STNOs are currently fabricated using the 50-nm technology where large arrays can be configured on a substrate. Each oscillator is independently isolated and unconnected at the fabrication stage. Once the devices are finished, the STNOs are bonded and connected in a series array. The postfabrication bonding and connection will afford us the opportunity to verify the results established in this paper.

ACKNOWLEDGMENTS

We acknowledge support from ONR Code 30. J.T. and A.P. were supported in part by NSF Grant No. CMMI-1068831. P.L.B. (Discovery Grant) and C.D. (USRA) acknowledge funding from NSERC Canada.

APPENDIX: HOPF CURVES

This appendix describes the mathematical analysis that was carried out to obtain the boundary curves that lead an array of STNO into and out of synchronization, as is shown in Fig. 2 in the main text. We start by considering again the array dynamics in stereographic coordinates captured by Eq. (3) with the full network in abbreviated form given by Eq. (4).

1. Linear analysis

Let $\mathbf{z}_0 = (z_0, \ldots, z_0)$ be an equilibrium solution of Eq. (4) with isotropy subgroup $\mathbf{S}_N$ [20]. Then, as described in the text, the linearization at $\mathbf{z}_0$ is given by

$$\mathbf{L} := \begin{bmatrix} \mathbf{A} & \mathbf{B} & \cdots & \mathbf{B} \\ \mathbf{B} & \ddots & \ddots & \vdots \\ \vdots & \ddots & \ddots & \mathbf{B} \\ \mathbf{B} & \cdots & \mathbf{B} & \mathbf{A} \end{bmatrix},$$

where $\mathbf{A} = (df_{jj})_{\mathbf{z}=\mathbf{z}_0}$ and $\mathbf{B} = (df_{jk})_{\mathbf{z}=\mathbf{z}_0}$ are 2×2 Jacobian matrices of f_j, with $j \neq k$. To diagonalize $\mathbf{L}$, we employ the $\mathbf{S}_N$ isotypic decomposition of the phase space $\mathbb{C}^N$, which is given by

$$\mathbb{C}^N = V_1 \oplus \mathbb{C}^{N,0},$$

where

$$V_1 = \{(z, \ldots, z) | z \in \mathbb{C}\},$$
$$\mathbb{C}^{N,0} = \{(z_1, \ldots, z_N) \in \mathbb{C}^N | \, z_1 + \cdots + z_N = 0\}$$

are absolutely irreducible representations of $\mathbf{S}_N$ [20]. Let

$$v_j = [v, \zeta^j v, \zeta^{2j} v, \ldots, \zeta^{(N-1)j} v]^T,$$

where $\zeta = \exp(2\pi i/N)$ and $v \in \mathbb{R}$. The vector v_0 is a basis for V_1 while the remaining vectors v_j, $j = 1, \ldots, N-1$, form a basis for $\mathbb{C}^{N,0}$. Now let

$$P = [\mathrm{Re}\{v_0\}, \mathrm{Im}\{v_0\}, \mathrm{Re}\{\bar{v_0}\}, \mathrm{Im}\{\bar{v_0}\}, \ldots,$$
$$\mathrm{Re}\{v_{N-1}\}, \mathrm{Im}\{v_{N-1}\}, \mathrm{Re}\{\bar{v}_{N-1}\}, \mathrm{Im}\{\bar{v}_{N-1}\}]^T.$$

Applying P to $\mathbf{L}$, we obtain the following block diagonalization of the linear part of the coupled STNO array:

$$\widetilde{\mathbf{L}} := P^{-1}\mathbf{L}P = \mathrm{diag}\{\mathbf{A} + (N-1)\mathbf{B}, \mathbf{A} - \mathbf{B}, \ldots, \mathbf{A} - \mathbf{B}\}. \tag{A1}$$

From the diagonal structure, the eigenvalues of the blocks are also eigenvalues of $\widetilde{\mathbf{L}}$. It follows that Hopf bifurcations in Eq. (4) occur if and only if $\mathbf{A} + (N-1)\mathbf{B}$ or $\mathbf{A} - \mathbf{B}$ have purely imaginary eigenvalues. In the former case, the eigenspace associated with $\mathbf{A} + (N-1)\mathbf{B}$ is

$$v_0 = [v, \ldots, v]^T,$$

where the symmetry group $\mathbf{S}_N$ acts trivially. This corresponds to a symmetry-preserving Hopf bifurcation in which all STNOs oscillate in synchrony, i.e., with the same wave form, the same amplitude, and the same phase. In the latter case, the eigenvalues have, generically, multiplicity $N-1$ (from the $N-1$ blocks $\mathbf{A} - \mathbf{B}$) and the emerging patterns of oscillations arise via symmetry-breaking Hopf bifurcations [20]. Combining the equilibrium conditions with the trace condition of purely imaginary eigenvalues for the block $\mathbf{A} + (N-1)\mathbf{B}$ (or equivalently $\mathbf{A} - \mathbf{B}$ for symmetry-breaking Hopf bifurcation) and using polar coordinates, $z_0 = r(\cos\theta + i\sin\theta)$, we get the following set of equations as a function of $(r, \cos\theta, I_{\mathrm{dc}}, \theta_h)$:

$$\begin{aligned} \mathrm{Re}(f_j) &= 0, \\ \mathrm{Im}(f_j) &= 0, \\ \mathrm{Tr}(\mathbf{A} + (N-1)\mathbf{B}) &= 0 \end{aligned} \tag{A2}$$

and require

$$\begin{aligned} \mathrm{Tr}(\mathbf{A} - \mathbf{B}) &< 0, \\ \det(\mathbf{A} - \mathbf{B}) &> 0, \\ \det(\mathbf{A} + (N-1)\mathbf{B}) &> 0, \end{aligned}$$

on the solution set of Eqs. (A2) to guarantee no eigenvalues with positive real parts. To find the desired analytical expressions for the Hopf boundary curves, we solve Eqs. (A2) implicitly for the state variables (r,θ) as functions of the parameters I_{dc} and θ_h. We set $N_1 = N_2 = 0.5$ as a starting point to facilitate analysis. Through a series of substitutions we are able to reduce this system of three equations with four unknowns, $(r,\theta,I_{\mathrm{dc}},\theta_h)$, to a single expression with two variables (r,θ_h). Using MAPLE's `implicitplot` function 16 times, curves are found in the (r,θ_h) domain to account for all possible solutions. Combining results produces the desired zero solution set of Eqs. (A2). To plot the Hopf curves, we first extract the coordinate points from the solution sets, and back-substituting gives the actual point values (I_{dc},θ) along the curves. Then we substitute these points to verify that $\det(\mathbf{A} - \mathbf{B}) > 0$ and $\det(\mathbf{A} + (N-1)\mathbf{B}) > 0$. By varying N in the implicit solver, we are then able to trace the movement of the synchronous Hopf bifurcation curves. As mentioned above, the Hopf curves are extended using AUTO to the case $N_1 = 1$, $N_2 = N_3 = 0$, and those are the curves plotted in Fig. 2.

2. Nonlinear analysis

We set again $N_1 = N_2 = 0.5$ as a starting point and assume $\mathbf{A} + (N-1)\mathbf{B}$ has a pair of purely imaginary eigenvalues and translate the equilibrium z_0 of Eq. (4) to the origin using $\mathbf{v} = \mathbf{z} - \mathbf{z}_0$, leading to

$$\dot{\mathbf{v}} = \mathbf{f}(\mathbf{v} + \mathbf{z}_0),$$

where f_j is given by

$$f_j = \frac{\gamma(1+i\alpha)}{1+\alpha^2}\Bigg[ih_{a3}(v_j+z_0)+\frac{h_{a2}}{2}(1+(v_j+z_0)^2) + i\kappa\frac{1-|v_j+z_0|^2}{1+|v_j+z_0|^2}(v_j+z_0)-\mu I_{\rm dc}(v_j+z_0) - \mu I_{\rm dc}\beta_{\Delta R}\sum_{k=1}^{N}\frac{1-|v_k+z_0|^2}{1+|v_k+z_0|^2}(v_j+z_0) + \frac{2\pi i S_0}{1+|v_j+z_0|^2}(v_j+z_0-(v_j+z_0)|v_j+z_0|^2)\Bigg]. \tag{A3}$$

To determine criticality of the Hopf bifurcation we set $g(v,\overline{v}) = (1+|v+z_0|^2)^{-1}$ and Taylor expand Eq. (A3) at (0,0) up to cubic order [30], which yields

$$\dot{v}_j = H_1(v_j,\overline{v}_j,v,\overline{v}) + \mathcal{N}(v_j,\overline{v}_j,v,\overline{v}), \tag{A4}$$

where $\mathcal{N}(v_j,\overline{v}_j,v,\overline{v}) = H_2(v_j,\overline{v}_j,v,\overline{v}) + H_3(v_j,\overline{v}_j,v,\overline{v})$ with H_ℓ a homogeneous polynomial of degree ℓ. That is,

$$\begin{aligned}
H_1(v,\overline{v}) &= a_{10}v_j + a_{01}\overline{v}_j + \sum_{k=1}^{n} b_{10}v_k + b_{01}\overline{v_k},\\
H_2(v,\overline{v}) &= a_{20}v_j^2 + a_{11}|v_j|^2 + a_{02}\overline{v}_j^2 + \sum_{k=1}^{n} b_{20}v_k^2 \\
&\quad + b_{11}|v_k|^2 + b_{02}\overline{v}_k + c_{110}v_jv_k + c_{101}v_j\overline{v}_k,\\
H_3(v,\overline{v}) &= a_{30}v_j^3 + a_{21}|v_j|^2v_j + a_{12}|v_j|^2\overline{v}_j + a_{03}\overline{v}_j^3 \\
&\quad + \sum_{k=1}^{n} b_{30}v_k^3 + b_{21}|v_k|^2v_k + b_{12}|v_k|^2\overline{v}_k + b_{03}\overline{v}_k^3 \\
&\quad + \left(c_{120}v_k^2 + c_{111}|v_k|^2 + c_{102}\overline{v}_k^2\right)v_j.
\end{aligned}$$

For brevity, we list only a few of the coefficients:

$$\begin{aligned}
b_{10}\tau &= \mu I_{\rm dc}\beta_{\Delta R}(2g(0,0)^2|z_0|^2),\\
a_{10}\tau &= ih_{a3} + z_0h_{a2} + i\kappa g(0,0)^2(1-2|z_0|^2-|z_0|^4) - \mu I_{\rm dc}\\
&\quad -\mu I_{\rm dc}\beta_{\Delta R}g(0,0)^2(N(1-|z_0|^4)-2|z_0|^2)\\
&\quad + 2\pi i S_0 g(0,0)^2(1-2|z_0|^2-|z_0|^4) - b_{10}\tau,\\
b_{11}\tau &= -2\mu I_{\rm dc}\beta_{\Delta R}z_0(|z_0|^2-1)g(0,0)^3,\\
c_{101}\tau &= 2\mu I_{\rm dc}\beta_{\Delta R}z_0 g(0,0)^2,\\
a_{11}\tau &= -4z_0g(0,0)^3\left(i\kappa + \frac{i}{2} - \mu I_{\rm dc}\beta_{\Delta R}\right) - b_{11}\tau - c_{101}\tau,
\end{aligned}$$

where $\tau = (1+\alpha^2)/(\gamma(1+i\alpha))$.

We now rewrite Eq. (A4) using the same matrix P given by the decomposition of $\mathbb{C}^N = \mathbb{C}^{N,0}\bigoplus V_1$ into $\mathbf{S}_N$ irreducible representations and letting $v = Pu$, yielding

$$\dot{u} = \widetilde{\mathbf{L}}u + P^T\mathbf{N}(Pu,\overline{Pu}),$$

where $\widetilde{\mathbf{L}} = P^T\mathbf{L}P$ are the linear terms given by Eq. (A1) and the nonlinear terms are $\mathbf{N}(v,\overline{v}) = (\mathcal{N}(v_1,\overline{v}_1,v,\overline{v}),\ldots,\mathcal{N}(v_N,\overline{v}_N,v,\overline{v}))^T$.

An important observation is that the center manifold is $V_1 = \mathrm{Fix}(\mathbf{S}_N)$ and so the flow-invariant center manifold is in fact a subspace for Eq. (4). Thus we can compute the criticality of the Hopf bifurcation directly from the equation for $\dot{u}_1$ evaluated at $u_\ell = \overline{u}_\ell = 0$ for $\ell = 2,\ldots,N$, which yields

$$\begin{aligned}
\dot{u}_1 &= G_{10}u_1 + G_{01}\overline{u_1} + G_{20}u_1^2 + G_{11}|u_1|^2 + G_{02}\overline{u}_1^2\\
&\quad + G_{30}u_1^3 + G_{21}|u_1|^2u_1 + G_{12}|u_1|^2\overline{u}_1 + G_{03}\overline{u}_1^3,
\end{aligned} \tag{A5}$$

where

$$\begin{aligned}
G_{10} &= a_{10} + Nb_{10},\\
G_{01} &= a_{01} + Nb_{01},\\
G_{20} &= [a_{20} + N(b_{20}+c_{110})]/\sqrt{N},\\
G_{11} &= [a_{11} + N(b_{11}+c_{101})]/\sqrt{N},\\
G_{02} &= (a_{02} + Nb_{02})/\sqrt{N},\\
G_{30} &= [a_{30} + \sqrt{N}(b_{30}+c_{120})]/\sqrt{N},\\
G_{21} &= [a_{21} + \sqrt{N}(b_{21}+c_{111})]/\sqrt{N},\\
G_{12} &= [a_{12} + \sqrt{N}(b_{12}+c_{102})]/\sqrt{N},\\
G_{03} &= (a_{03} + \sqrt{N}b_{03})/\sqrt{N}.
\end{aligned}$$

Now, at a Hopf bifurcation, $\mathrm{Re}(G_{10}) = 0$ and the eigenvalues are $\pm i\rho$ with

$$\rho := \sqrt{|G_{10}|^2 - |G_{01}|^2}.$$

We use the linear transformation

$$Q = \begin{pmatrix} G_{01} & i\mathrm{Im}(G_{10}) - i\rho \\ -i\mathrm{Im}(G_{10}) + i\rho & \overline{G}_{01}\end{pmatrix}$$

and the change of coordinates $[w_1,\bar{w}_1] = Q[u_1,\bar{u}_1]^T$ to diagonalize the linear part of Eq. (A5) to $\mathrm{diag}(i\rho,-i\rho)$. Let $\widetilde{H}_\ell(w_1,\overline{w}_1) = Q^{-1}H_\ell(Q(w_1,\overline{w}_1)^T)$ for $\ell = 2,3$, then

$$\begin{aligned}
\dot{w}_1 &= i\rho w_1 + \frac{\rho + \mathrm{Im}(G_{10})}{2G_{01}\rho}(\widetilde{H}_2(w_1,\overline{w}_1) + \widetilde{H}_3(w_1,\overline{w}_1))\\
&\quad - \frac{i}{2\rho}(\overline{\widetilde{H}_2(w_1,\overline{w}_1)} + \overline{\widetilde{H}_3(w_1,\overline{w}_1)}).
\end{aligned} \tag{A6}$$

We denote by g_{ij} the coefficients of the quadratic and cubic terms; $i+j=\ell$ and $\ell = 2,3$. For the quadratic terms, the coefficients are

$$\begin{aligned}
g_{20} &= \frac{[\rho + \mathrm{Im}(G_{10})]}{2G_{01}\rho}\left[4G_{20}G_{01}^2 + G_{11}(-2G_{10}G_{01}i + 2iG_{01}\rho)\right.\\
&\quad \left. + G_{02}\left(-G_{10}^2 + 2G_{10}\rho - \rho^2\right)\right]\\
&\quad - \frac{i}{2\rho}\left(\overline{4G_{20}G_{01}^2 + G_{11}(-2G_{10}G_{01}i + 2iG_{01}\rho)}\right.\\
&\quad \left. + \overline{G_{02}\left(-G_{10}^2 + 2G_{10}\rho - \rho^2\right)}\right),\\
g_{11} &= \frac{[\rho + \mathrm{Im}(G_{10})]}{2G_{01}\rho}\left[8G_{20}G_{01}^2 + G_{11}(-4G_{10}G_{01}i)\right.\\
&\quad \left. + G_{02}\left(-2G_{10}^2 + 2\rho^2\right)\right]\\
&\quad - \frac{i}{2\rho}\left(\overline{8G_{20}G_{01}^2 + G_{11}(-4G_{10}G_{01}i)}\right.\\
&\quad \left. + \overline{G_{02}\left(-2G_{10}^2 + 2\rho^2\right)}\right),
\end{aligned}$$

$$g_{02} = \frac{[\rho + \mathrm{Im}(G_{10})]}{2G_{01}\rho}\big[4G_{20}G_{01}^2 + G_{11}(-2G_{10}G_{01}i - 2iG_{01}) + G_{02}\big(-G_{10}^2 - 2G_{10}\rho - \rho^2\big)\big] - \frac{i}{2\rho}\big(\overline{4G_{20}G_{01}^2 + G_{11}(-2G_{10}G_{01}i - 2iG_{01})} + \overline{G_{02}\big(-G_{10}^2 - 2G_{10}\rho - \rho^2\big)}\big),$$

and the cubic coefficient is

$$g_{21} = \frac{[\rho + \mathrm{Im}(G_{10})]}{2G_{01}\rho}W - \frac{i}{2\rho}\overline{W},$$

where

$$W := \big\{12G_{30}G_{01}^3 + G_{21}\big(-6G_{10}G_{01}^2 i + 2iG_{01}^2\rho\big) + G_{12}[4G_{10}G_{01}(-G_{10} + \rho) - 2G_{10}(G_{10} - \rho)] + 2G_{01}\rho(G_{10} + \rho) + G_{03}\big[\big(G_{10}^2 - 2G_{10}\rho + \rho^2\big)(G_{10} + \rho)i + 2i(\rho^2 - G_{10}^2)(-G_{10} + \rho)\big]\big\}.$$

3. Lyapunov constant and stability

Using the coefficients just listed above, we then obtain the Lyapunov constant from the formula [30]

$$\mathrm{Re}(c_1) = \mathrm{Re}\left(\frac{i}{2\rho}\left(g_{20}g_{11} - 2|g_{11}|^2 - \frac{1}{3}|g_{02}|^2\right) + \frac{g_{21}}{2}\right). \tag{A7}$$

The Hopf bifurcation is supercritical if $\mathrm{Re}(c_1) < 0$ and subcritical if $\mathrm{Re}(c_1) > 0$. However, this condition only determines the stability of the synchronized periodic solution on the center manifold. Thus, we also need to consider the eigenvalues transverse to the center manifold. Those eigenvalues are given by $N - 1$ copies of the eigenvalues of the block $\mathbf{A} - \mathbf{B}$ with real parts $\frac{1}{2}\,\mathrm{Tr}(\mathbf{A} - \mathbf{B}) = \mathrm{Re}(a_{10} - b_{10})$. It follows that the synchronized oscillations are asymptotically stable if $\mathrm{Re}(a_{10} - b_{10}) < 0$.

For $N_1 = N_2 = 0.5$, subcritical Hopf bifurcations are obtained. We change the direction of demagnetization to $N_1 = 1$, $N_2 = N_3 = 0$ by numerical continuation using AUTO and we obtain that Hopf bifurcation curves in the first quadrant of $(I_{\mathrm{dc}},\theta_h)$ space are supercritical and the synchronization manifold is asymptotically stable near z_0. This leads to an asymptotically stable periodic solution near bifurcation. See Fig. 2.

[1] J. Grollier, V. Cros, and A. Fert, Phys. Rev. B **73**, 060409(R) (2006).
[2] S. Kaka, M. R. Pufall, W. H. Rippard, T. J. Silva, S. E. Russek, and J. A. Katine, Nat. Lett. **437**, 389 (2005).
[3] J. Persson, Y. Zhou, and J. Akerman, J. Appl. Phys. **101**, 09A503 (2007).
[4] R. Adler, Proc. IEEE **61**, 1380 (1973).
[5] Z. Li, Y. C. Li, and S. Zhang, Phys. Rev. B **74**, 054417 (2006).
[6] B. Georges, J. Grollier, M. Darques, V. Cros, C. Deranlot, B. Marcilhac, G. Faini, and A. Fert, Phys. Rev. Lett. **101**, 017201 (2008).
[7] V. Tiberkevich, A. Slavin, E. Bankowski, and G. Gerhart, Appl. Phys. Lett. **95**, 262505 (2009).
[8] S. Urazhdin, P. Tabor, V. Tiberkevich, and A. Slavin, Phys. Rev. Lett. **105**, 104101 (2010).
[9] B. Subash, V. K. Chandrasekar, and M. Lakshmanan, Europhys. Lett. **109**, 17009 (2015).
[10] A. Houshang, E. Iacocca, P. Durrenfeld, S. R. Sani, J. Akerman, and R. K. Dumas, Nat. Nanotechnol. **11**, 280 (2016).
[11] T. Kendziorczyk, S. O. Demokritov, and T. Kuhn, Phys. Rev. B **90**, 054414 (2014).
[12] B. Georges, J. Grollier, V. Cros, and A. Fert, Appl. Phys. Lett. **92**, 232504 (2008).
[13] Y. Kuramoto, in *Proceedings of the International Symposium on Mathematical Problems in Theoretical Physics*, edited by H. Araki, Lecture Notes in Physics Vol. 39 (Springer, Berlin, 1975).
[14] E. Iacocca and J. Akerman, J. Appl. Phys. **110**, 103910 (2011).
[15] M. G. Rosenblum, A. S. Pikovsky, and J. Kurths, Phys. Rev. Lett. **78**, 4193 (1997).
[16] Z. Zeng, G. Finocchio, and H. Jiang, Nanoscale **5**, 2219 (2013).
[17] L. V. Gambuzza, J. Gomez-Gardenes, and M. Frasca, Sci. Rep. **6**, 24915 (2016).
[18] F. B. Mancoff, N. D. Rizzo, B. N. Engel, and S. Tehrani, Nat. Lett. **437**, 393 (2005).
[19] D. Li, Y. Zhou, C. Zhou, and B. Hu, Phys. Rev. B **82**, 140407 (2010).
[20] M. Golubitsky, I. N. Stewart, and D. G. Schaeffer, *Singularities and Groups in Bifurcation Theory Vol. II* (Springer-Verlag, New York, 2004), Vol. 69.
[21] S. Murugesh and M. Lakshmanan, Chaos, Solitons Fractals **41**, 2773 (2009).
[22] N. Fenichel, Indiana Univ. Math. J. **21**, 193 (1971).
[23] M. W. Hirsch, C. C. Pugh, and M. Shub, *Invariant Manifolds*, Lecture Notes in Physics Vol. 583 (Springer-Verlag, New York, 1977).
[24] D. Li, Y. Zhou, B. Hu, J. Akerman, and C. Zhou, Phys. Rev. B **86**, 014418 (2012).
[25] L. Berger, Phys. Rev. B **54**, 9353 (1996).
[26] M. Lakshmanan and K. Nakamura, Phys. Rev. Lett. **53**, 2497 (1984).
[27] M. Lakshmanan, Philos. Trans. R. Soc. **369**, 1280 (2011).
[28] C. S. Liu, K. C. Chen, and C. S. Yeh, J. Marine Sci. Technol -Taiwan **17**, 228 (2009).
[29] E. J. Doedel, Congr. Numer. **30**, 265 (1981).
[30] Y. Kuznetsov, *Elements of Applied Bifurcation Theory* (Springer-Verlag, New York, 1988).
[31] P. S. Skardal and A. Arenas, Sci. Adv. **1**, e1500339 (2015).
[32] J. Turtle, K. Beauvais, R. Shaffer, A. Palacios, V. In, T. Emery, and P. Longhini, J. Appl. Phys. **113**, 114901 (2013).
[33] H. Q. Cui, L. Cai, L. Ni, P. Wei, C. W. Feng, and X. K. Yang, J. Supercond. Novel Magn. **29**, 2873 (2016).
[34] A. Slavin and V. Tiberkevich, IEEE Trans. Magn. **45**, 1875 (2009).
[35] Z. Zeng, P. K. Amiri, I. N. Krivorotov, H. Zhao, G. Finocchio, J. P. Wang, J. A. Katine, Y. Huai, J. Langer, K. Galatsis, K. L. Wang, and H. W. Jiang, ACS Nano **6**, 6115 (2012).